IET Generation, Transmission & Distribution

Research Article

IET Journals
The Institution of Engineering and Technology

Approach to determine harmonic contributions in distribution networks using underdetermined blind source separation and form similarity distance

ISSN 1751-8687
Received on 17th November 2019
Revised 14th February 2020
Accepted on 2nd March 2020
E-First on 3rd June 2020
doi: 10.1049/iet-gtd.2019.1731
www.ietdl.org

Tong Ding[1], Hongkun Chen[1] ✉, Pan Hu[2], Lei Chen[1]

[1]*School of Electrical Engineering and Automation, Wuhan University, Wuhan, People's Republic of China*

[2]*State Grid Hubei Electric Power Research Institute, Wuhan, People's Republic of China*

✉ *E-mail: chkinsz@163.com*

Abstract: This study proposes a new approach to determine harmonic contributions in distribution networks. The approach effectively combines underdetermined blind source separation (UBSS) and form similarity distance (FSD), and it aims to minimise the negative impacts of harmonic source coupling and background harmonic fluctuations. Considering the underdetermined measurement, UBSS is introduced to estimate the harmonic emission current in the light of the sparsity of source signals. Through analysing the form variation features of harmonic time series, FSD is applied to identify the relatively stable background harmonics for utility equivalent harmonic impedance calculation. Furthermore, a complete procedure of harmonic contribution assessment is presented. To verify the high performance of the proposed approach, the simulation study and field test are both conducted, and a detailed comparative analysis of different approaches is carried out. The results show that the proposed approach is able to more accurately determine harmonic contributions than the existing methods, and has better robustness against significant harmonic source coupling and drastic background harmonic fluctuations.

1 Introduction

1.1 Motivation

The penetration rate of power electronic-interfaced distributed generations (DGs) and non-linear loads has been increasing in distribution networks. This results in voltage and current distortion and the more serious harmonic pollution, which threatens the safe, stable, and economical operation of power systems [1–4]. To efficiently mitigate harmonics and avoid power quality disputes between the power supplier and customers, an incentive-punishment mechanism is proposed [5], but the necessary prerequisite for the implementation is to appropriately determine harmonic contributions of harmonic sources.

1.2 Literature review and existing problems

Various works have been conducted to develop effective methods for harmonic contribution determination, which can be mainly classified as multipoint approaches and single-point approaches [6]. Multipoint approaches focus on the harmonic impact of multiple harmonic sources on a concerned busbar [7, 8]. The key to this technique is to achieve synchronous measurements of voltages and currents at different nodes of power networks, but the demand for complex and costly measurement devices leads to a limited practical application. In contrast, single-point approaches are easier to implement and more cost-effective. They pay attention to assessing the utility and customer harmonic contributions to the point of common coupling (PCC), in which the accurate estimation of the harmonic emission current and utility harmonic impedance are two critical steps. In terms of existing research studies, considering the inconvenience of obtaining the harmonic emission current, the measured branch harmonic current is usually used instead. In addition, for the utility harmonic impedance calculation, the non-invasive methods are generally adopted, such as the fluctuation method [9], data correlation analysis [10], and independent random vectors [11].

However, harmonics in modern distribution networks present some new features compared with traditional distribution networks, and there are two main challenging issues for harmonic contribution determination as follows:

(i) Harmonic coupling effect: large-scale distributed harmonic sources are integrated into distribution networks, which causes the increasingly significant harmonic coupling effect. The branch harmonic current is the product of the interaction of harmonic sources, while the harmonic emission current is generated under the rated power supply condition due to the inherent distortion characteristics. Thus, the branch harmonic current is evidently different from the harmonic emission current and fails to indicate the actual impact on harmonic distortion. As a result, the assessment errors will be inevitably caused in the light of existing methods.

Since the harmonic emission current is only related to the load characteristics and operation status of each harmonic source, it can be considered independent of each other, thus satisfying the premise of blind source separation. This technique is competent to recover source signals from multiple mixed observed signals even without any prior knowledge. The existing classical algorithms, such as independent component analysis and approximate joint diagonalisation [12, 13], usually demand that the number of observed signals should not be less than the number of source signals. Nevertheless, it is sometimes unable to meet the requirement because underdetermined situations may occur in practical projects, which are resulted from the limitation of measurement equipment and the existence of unknown harmonic sources. The above classical methods are not applicable to the problem of insufficient measurements, so it is crucial to find a feasible way to overcome the harmonic coupling effect for harmonic emission current estimation under underdetermined conditions.

(ii) Background harmonic fluctuations: the intermittence and randomness of new harmonic sources such as DGs and electric vehicles make the dynamic time-varying feature of background harmonics in modern distribution networks more obvious. The conventional non-invasive methods are susceptible to background harmonic variations, which will affect the performance of utility harmonic impedance calculation.

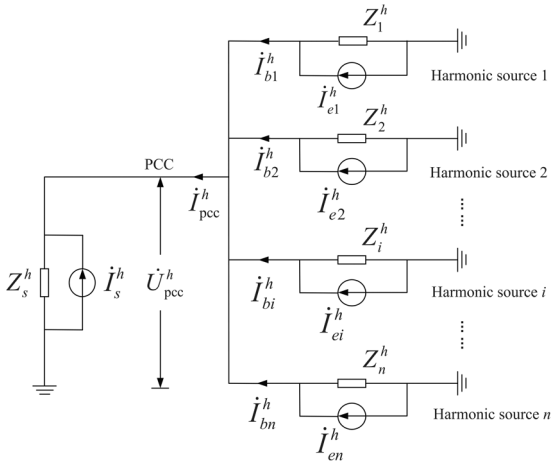

Fig. 1 *Norton equivalent circuit of the distribution network with multiple harmonic sources*

In terms of alleviating the negative impacts of background harmonic fluctuations, it is reliable to select the time interval with stable background harmonics for utility harmonic impedance calculation. Given the fact that the harmonic voltage at the PCC and the harmonic emission current of the concerned harmonic source show the same or opposite variation trend when the background harmonic is constant, the time series similarity is suitable for searching the synchronous fluctuation information to identify the relatively stable background harmonics. This technique only requires the harmonic voltage and current amplitudes, so it owns the advantage of easy implementation in practice. Euclidean distance and dynamic time warping (DTW) distance are two common methods for similarity search [14, 15], but both methods focus too much on the similarity of data values and overlook the form variation trend of time series, which leads to certain deficiencies in evaluating the similarity degree between a pair of time series with diverse data values but similar form features. Therefore, a more efficient method for the form similarity search of time series is required to calculate the utility harmonic impedance.

1.3 Contributions

This study presents a novel approach for harmonic contribution determination in distribution networks. Two technical issues, the harmonic emission current estimation of coupled harmonic sources and the utility equivalent harmonic impedance calculation under significant background harmonic fluctuations, are taken into consideration. The solutions are derived from underdetermined blind source separation (UBSS) and form similarity distance (FSD), respectively. The performance of the proposed approach is verified by numerical simulation and field measurement. The results of the comparative analysis show better effectiveness and suitability of the proposed approach. The main contributions of this study are as follows:

(i) Introduce an UBSS-based method to eliminate the coupling effect of harmonic sources for harmonic emission current estimation considering the underdetermined measurement.
(ii) Apply a FSD-based method to alleviate the adverse impact of background harmonic fluctuations on utility equivalent harmonic impedance calculation considering the form features of time series.
(iii) Design a complete process of harmonic contribution determination, which is validated by the comparative analysis with the existing methods.

1.4 Paper organisation

The rest of this paper is organised as follows. Section 2 introduces the main problems of existing methods for harmonic contribution determination. In Sections 3 and 4, based on UBSS and FSD, respectively, the solutions are presented from harmonic emission current estimation and utility equivalent harmonic impedance calculation. Section 5 elaborates on the complete procedure for determining harmonic contributions. The performance of the proposed approach is verified by a simulation study and field measurement in Sections 6 and 7. Finally, the main conclusions are summarised in Section 8.

2 Problem description

In a regional distribution network, there are multiple harmonic sources connected to the PCC, which can be regarded as the Norton equivalent circuit, as illustrated in Fig. 1. Z_s^h and $\dot{I}_s^h$ denote the hth equivalent harmonic impedance and harmonic current source of the utility side, respectively. Z_i^h and $\dot{I}_{ei}^h$ denote the hth equivalent harmonic impedance and harmonic emission current of harmonic source i, respectively, where $i = 1, 2, \ldots, n$. $\dot{I}_{bi}^h$ is the hth branch harmonic current of harmonic source i.

The harmonic voltage projection method based on the vector superposition principle is widely applied to determine harmonic contributions of harmonic sources to the distortion at the PCC [16–18]. Assuming that there are k sampling points in the concerned time interval, the hth harmonic contribution of harmonic source i at the lth sampling point is denoted as $\mu_{pcc\_i}^h(l)$, which is defined as

$$\begin{aligned}\mu_{pcc\_i}^h(l) &= \frac{\left|\dot{U}_{pcc\_i}^h\right|(l)\cos\theta_i(l)}{\left|\dot{U}_{pcc}^h\right|(l)} \times 100\% \\ &= \frac{\left|\dot{I}_{ei}^h\right|(l)\left|\dot{Z}_{pcc\_i}^h\right|\cos\theta_i(l)}{\left|\dot{U}_{pcc}^h\right|(l)} \times 100\%\end{aligned} \tag{1}$$

where $|\bullet|(l)$ denotes the amplitude data at the lth sampling point and $l = 1, 2, \ldots, k$. $\dot{U}_{pcc}^h$ denotes the hth harmonic voltage at the PCC. $\dot{U}_{pcc\_i}^h$ denotes the hth harmonic voltage produced by harmonic source i. $\dot{Z}_{pcc\_i}^h$ denotes the hth harmonic impedance at the PCC except for harmonic source i. $\cos\theta_i$ denotes the cosine value of the phase angle between $\dot{U}_{pcc}^h$ and $\dot{U}_{pcc\_i}^h$, which may be positive or negative, indicating that harmonic source i promotes or mitigates the hth harmonic voltage at the PCC, respectively.

The hth average harmonic contribution of harmonic source i during the concerned time interval is denoted as $\mu_{pcc\_i}^h$, which can be calculated as

$$\mu_{pcc\_i}^h = \frac{\sum_{l=1}^{k} \mu_{pcc\_i}^h(l)}{k} \tag{2}$$

Derived from (1), since $\left|\dot{U}_{pcc}^h\right|$ can be measured directly at the PCC, the keys to evaluating the harmonic contribution are to determine $\left|\dot{I}_{ei}^h\right|$, $\left|\dot{Z}_{pcc\_i}^h\right|$, and $\cos\theta_i$.

As for $\left|\dot{I}_{ei}^h\right|$, it fails to be collected by field measurements, so the branch harmonic current $\left|\dot{I}_{bi}^h\right|$ is commonly adopted for approximate analysis in most research studies. Nevertheless, due to the harmonic coupling effect, $\dot{I}_{bi}^h$ is generated not only by harmonic source i but also by the harmonic voltage produced by other harmonic sources at the PCC. According to Kirchhoff's current law, $\dot{I}_{bi}^h$ can be determined as

$$\dot{I}_{bi}^h = \dot{I}_{ei}^h - \sum_{i'=1, i' \neq i}^{n} \dot{I}_{i\_i'}^h - \dot{I}_{i\_0}^h \tag{3}$$

where $\dot{I}_{i\_0}^h$ denotes the hth branch harmonic current on the ith feeder caused by the utility harmonic source and $\dot{I}_{i\_i'}^h$ denotes the hth branch harmonic current on the ith feeder caused by the customer harmonic source $i'(i' = 1, 2, \ldots, n,\ i' \neq i)$.

The phasor relationship among the above harmonic currents is illustrated in Fig. 2. From the figure, there is an obvious deviation

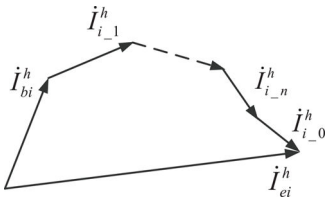

Fig. 2 *Phasor relationship among harmonic currents*

between $\dot{I}^h_{bi}$ and $\dot{I}^h_{ei}$. Hence, it is necessary to estimate the harmonic emission current for the improvement of assessment accuracy.

In terms of the calculation of $\left|Z^h_{pcc\_i}\right|$, the conventional non-invasive methods are sensitive to background harmonic fluctuations. Moreover, it is impractical to solve $\cos\theta_i$ directly because most power quality monitoring systems fail to collect the real-time harmonic phase angles in practical engineering. Aiming at these issues, researchers have presented that there is a linear correlation between $\left|\dot{U}^h_{pcc}\right|$ and $\left|\dot{I}^h_{ei}\right|$ under stable background harmonics [19]. In this case, the utility equivalent harmonic impedance $\left|\dot{Z}^h_{pcc\_i}\right|\cos\theta_i$ is regarded as the regression coefficient of the linear equation and determined as a whole by linear regression algorithms, but the premise of this approach is to properly identify the relatively stable background harmonics.

3 Harmonic emission current estimation

3.1 Corresponding relationships of the used models

In the model of blind source separation, the relation between the observed signals and the source signals is expressed as

$$\boldsymbol{x} = \boldsymbol{A}\boldsymbol{s} \tag{4}$$

where $\boldsymbol{x}$ denotes a column vector consisting of m observed signals. $\boldsymbol{s}$ denotes a column vector consisting of n unknown source signals that are statistically independent. $\boldsymbol{A}$ denotes a mixing matrix with $m \times n$ dimensions. When m is less than n, (4) represents the model of UBSS.

For the harmonic current estimation, the node harmonic voltage or the branch harmonic current is often regarded as the measured variable, and the harmonic emission current is taken as the state variable [20]. If the node harmonic voltage is chosen as the measured variable, the calculation of harmonic impedance will be involved, which is susceptible to many interference factors, so the branch harmonic current is to be measured in this study. The model for harmonic emission current estimation can accordingly be represented as

$$\boldsymbol{I}_\mathrm{b} = \boldsymbol{H}\boldsymbol{I}_\mathrm{e} \tag{5}$$

where $\boldsymbol{I}_\mathrm{b}$ denotes the branch harmonic current vector with $m \times 1$ dimensions, $\boldsymbol{I}_\mathrm{e}$ denotes the harmonic emission current vector with $n \times 1$ dimensions and $\boldsymbol{H}$ denotes the relation matrix with $m \times n$ dimensions.

In view of the finite measurements in practice, the number of measured variables is often less than that of state variables, and thus (5) is an underdetermined equation. By comparing (4) with (5), the corresponding relationship of the two models is shown as follows:

$$\begin{cases} \boldsymbol{x} \leftrightarrow \boldsymbol{I}_\mathrm{b} \\ \boldsymbol{A} \leftrightarrow \boldsymbol{H} \\ \boldsymbol{s} \leftrightarrow \boldsymbol{I}_\mathrm{e} \end{cases} \tag{6}$$

Therefore, the UBSS model enables harmonic source decoupling and harmonic emission current estimation under underdetermined measurements. The realisation of UBSS is mainly based on the sufficient sparsity of source signals, which means that the value of most source signals is zero or approaching zero at any sampling point [21]. The two-step method is widely adopted, in which the first step is to estimate the mixing matrix in the light of the observed signals, and in the second step, the source signals are recovered.

3.2 Mixing matrix estimation

The harmonic emission current signals are often inadequately sparse in practical situations, so the method for mixing matrix estimation under the condition of sufficient sparsity is unsuitable. It is helpful to transform observed signals from the time domain to the time-frequency domain for improving the sparsity. Short-time Fourier transform is one of the common time-frequency transform methods, but this technique has the defect of the fixed height and width of the used window function. Instead, *S*-transform introduces the Gaussian window whose height and width vary with frequency, which owns the advantage of multi-resolution, so it is adopted to pre-process the branch harmonic currents.

In the time-frequency domain, the relation between the branch harmonic current vector and the harmonic emission current vector is expressed as

$$\boldsymbol{I}_\mathrm{b}(t, f) = \boldsymbol{H}\boldsymbol{I}_\mathrm{e}(t, f) \tag{7}$$

According to the short-term stationary characteristic of non-stationary signals [22], there must be a time-frequency point where only one source signal plays the leading role, which is called the time-frequency single source point. Assuming the point $(t_\mathrm{p}, f_\mathrm{p})$ is a time-frequency single source point, where only the harmonic emission current $I_{ei}(t_\mathrm{p}, f_\mathrm{p})$ of harmonic source i is dominant, (7) can be rewritten as

$$\boldsymbol{I}_\mathrm{b}(t_\mathrm{p}, f_\mathrm{p}) = \boldsymbol{h}_i I_{ei}(t_\mathrm{p}, f_\mathrm{p}) \tag{8}$$

where $\boldsymbol{h}_i$ is the ith column vector of the mixing matrix $\boldsymbol{H}$.

The real part and the imaginary part of (8) are separated, then we have

$$\begin{cases} \mathrm{Re}\{\boldsymbol{I}_\mathrm{b}(t_\mathrm{p},\ f_\mathrm{p})\} = \boldsymbol{h}_i \mathrm{Re}\{I_{ei}(t_\mathrm{p},\ f_\mathrm{p})\} \\ \mathrm{Im}\{\boldsymbol{I}_\mathrm{b}(t_\mathrm{p},\ f_\mathrm{p})\} = \boldsymbol{h}_i \mathrm{Im}\{I_{ei}(t_\mathrm{p},\ f_\mathrm{p})\} \end{cases} \tag{9}$$

The angle between $\mathrm{Re}\{\boldsymbol{I}_\mathrm{b}(t_\mathrm{p},\ f_\mathrm{p})\}$ and $\mathrm{Im}\{\boldsymbol{I}_\mathrm{b}(t_\mathrm{p},\ f_\mathrm{p})\}$ is set to φ, which can be calculated as

$$\cos\varphi = \frac{\mathrm{Re}\{\boldsymbol{I}_\mathrm{b}(t_\mathrm{p},\ f_\mathrm{p})\}^\mathrm{T} \mathrm{Im}\{\boldsymbol{I}_\mathrm{b}(t_\mathrm{p},\ f_\mathrm{p})\}}{\| \mathrm{Re}\{\boldsymbol{I}_\mathrm{b}(t_\mathrm{p},\ f_\mathrm{p})\} \| \ \| \mathrm{Im}\{\boldsymbol{I}_\mathrm{b}(t_\mathrm{p},\ f_\mathrm{p})\} \|} \tag{10}$$

It is found that the absolute value of $\cos\varphi$ is equal to 1, indicating that $\mathrm{Re}\{\boldsymbol{I}_\mathrm{b}(t_\mathrm{p},\ f_\mathrm{p})\}$ and $\mathrm{Im}\{\boldsymbol{I}_\mathrm{b}(t_\mathrm{p},\ f_\mathrm{p})\}$ are in the same or opposite directions, which enables the identification of time-frequency single source points. In practice, the directions of the real part and imaginary part may not be exactly in a straight line because of the noise signals. The time-frequency point can be regarded as a single source point as long as the absolute value of $\cos\varphi$ is larger than a certain threshold value close to 1.

The set of all time-frequency single source points is called the time-frequency single source region, where the scatter points of observed signals are approximately located in several straight lines and show obvious aggregation, as indicated in Fig. 3. The direction vectors of straight lines correspond to the column vectors of the mixing matrix. For the purpose of improving the performance of mixing matrix estimation, the branch harmonic current vector is normalised firstly, then the clustering algorithm, such as fuzzy *C*-means clustering, is used to search the clustering centres, whose coordinates are the elements of the corresponding column vectors. Thus, all column vectors are estimated by the clustering centres and the entire mixing matrix is established.

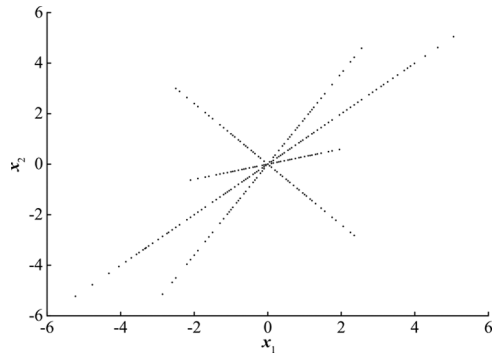

Fig. 3 *Scatter diagram of two observed signals in the time-frequency single source region*

3.3 Source signal recovery

The above mixing matrix is not a square matrix, so it is impossible to recover source signals by directly constructing the inverse matrix. The l_1 norm minimisation-based algorithm is usually introduced to handle the underdetermined equation [23], and the optimisation model shown as follows needs to be solved:

$$\begin{cases} \min\limits_{\boldsymbol{I}_{\mathrm{e}}(t,\,f)} \sum\limits_{i=1}^{n} |I_{\mathrm{e}i}(t,\,f)| \\ \mathrm{s.t.}\ \boldsymbol{I}_{\mathrm{b}}(t,\,f) = \boldsymbol{H}\boldsymbol{I}_{\mathrm{e}}(t,\,f) \end{cases} \tag{11}$$

The solution to the model is called the minimum l_1 norm solution, among which there are at most m non-zero values according to [24]. Hence, there are C_n^m possible solutions to (11), and the minimum value of all possible solutions is the optimal solution. The specific steps are as follows.

Step 1: C_n^m submatrices with $m \times m$ dimensions are extracted from the mixing matrix $\boldsymbol{H}$, denoted as $\boldsymbol{B}_k = [\boldsymbol{h}_{k_1},\ \boldsymbol{h}_{k_2}, \ldots, \boldsymbol{h}_{k_m}]$, where $k = 1, 2, \ldots, C_n^m$. Each column of submatrix $\boldsymbol{B}_k$ is the column vector of mixing matrix $\boldsymbol{H}$, so $k_1,\ k_2, \ldots, k_m \in [1,\ n]$.

Step 2: For the time-frequency single source point $(t_{\mathrm{p}}, f_{\mathrm{p}})$, one of the possible solutions to (11), denoted as $\hat{\boldsymbol{I}}_{\mathrm{e}}^{k}(t_{\mathrm{p}},\ f_{\mathrm{p}})$, can be determined as

$$\begin{cases} \hat{\boldsymbol{I}}_{\mathrm{e}}^{k}(t_{\mathrm{p}},\ f_{\mathrm{p}}) = \left[\hat{I}_{\mathrm{e}1}^{k}(t_{\mathrm{p}},\ f_{\mathrm{p}}), \ldots, \hat{I}_{\mathrm{e}n}^{k}(t_{\mathrm{p}},\ f_{\mathrm{p}})\right] \\ \left[\hat{I}_{\mathrm{e}k_1}^{k}(t_{\mathrm{p}},\ f_{\mathrm{p}}), \ldots,\ \hat{I}_{\mathrm{e}k_m}^{k}(t_{\mathrm{p}},\ f_{\mathrm{p}})\right]^{\mathrm{T}} = \boldsymbol{B}_k^{-1}\boldsymbol{I}_{\mathrm{b}}(t_{\mathrm{p}},\ f_{\mathrm{p}}) \\ \hat{I}_{\mathrm{e}j}^{k}(t_{\mathrm{p}},\ f_{\mathrm{p}}) = 0,\ j \in [1,\ n],\ j \neq k_1,\ k_2, \ldots, k_m \end{cases} \tag{12}$$

Step 3: The l_1 norm J_k of $\hat{\boldsymbol{I}}_{\mathrm{e}}^{k}(t_{\mathrm{p}},\ f_{\mathrm{p}})$ can be determined as

$$J_k = \sum_{i=1}^{n} \left|\hat{I}_{\mathrm{e}i}^{k}(t_{\mathrm{p}},\ f_{\mathrm{p}})\right|, \quad k = 1, 2, \ldots, C_n^m \tag{13}$$

Step 4: For all C_n^m possible solutions, the l_1 norm is calculated in turn by (13) and a comparison is carried out. The possible solution corresponding to the minimum l_1 norm is taken as the estimated value $\hat{\boldsymbol{I}}_{\mathrm{e}}(t_{\mathrm{p}},\ f_{\mathrm{p}})$ of the harmonic emission current at the point $(t_{\mathrm{p}}, f_{\mathrm{p}})$, which is expressed as

$$\hat{\boldsymbol{I}}_{\mathrm{e}}(t_{\mathrm{p}},\ f_{\mathrm{p}}) = \min_{\hat{\boldsymbol{I}}_{\mathrm{e}}^{k}(t_{\mathrm{p}},\, f_{\mathrm{p}})} J_k, \quad k = 1,\ 2, \ldots, C_n^m \tag{14}$$

Step 5: All time-frequency single source points are processed successively according to steps 2–4, and the harmonic emission current $\boldsymbol{I}_{\mathrm{e}}(t, f)$ in the time-frequency domain is determined. The time-domain form $\boldsymbol{I}_{\mathrm{e}}(t)$ can be recovered by inverse S-transform.

4 Utility equivalent harmonic impedance calculation

It is necessary to reduce the undesirable influence of background harmonic variations for the precise calculation of the harmonic impedance. For this purpose, the FSD-based method is designed to select the time series of harmonic voltage amplitudes and harmonic emission current amplitudes with high form similarity through analysing the form variation characteristics. Thus, the data segment with relatively stable background harmonics is identified for determining the utility equivalent harmonic impedance.

4.1 Identification of key trend turning points

The harmonic data sampled by power quality monitoring devices are a series of time-dependent values, which is denoted as the time series $X = [(t_1, x_1), (t_2, x_2), \ldots, (t_m, x_m)]$. x_i represents the harmonic data at time t_i, where $i = 1, 2, \ldots, m$ and m is the length of X. The variation trends of time series are generally classified into three forms: rising, stationary, and falling. The joint points of different forms are called the trend turning points, the identification of which is helpful to distinguish the local variations of time series, but there is a considerable workload. Besides, some trend turning points fail to reflect important form features due to noise signals and other interference factors, so it is necessary to conduct further screening to confirm the key trend turning points that contain significant information of form variation.

The time span and vertical distance are introduced to identify the key trend turning points considering two factors of the time dimension and the numerical dimension [25]. Assuming that (t_{i-1}, x_{i-1}), (t_i, x_i), and (t_{i+1}, x_{i+1}) are three successive trend turning points of the time series X, the time span t and the vertical distance d from the point (t_i, x_i) to adjacent two points are, respectively, defined as

$$t = \min\{t_i - t_{i-1},\ t_{i+1} - t_i\} \tag{15}$$

$$d = \left| x_{i-1} - x_i + \frac{(x_{i+1} - x_{i-1})(t_i - t_{i-1})}{t_{i+1} - t_{i-1}} \right| \tag{16}$$

The point (t_i, x_i) is regarded as the key trend turning point when t and d exceed the specified threshold, which is set according to the magnitude and length of time series. The harmonic time series is segmented into several sub-sequences by the key trend turning points, and there are almost uniform form features within each subsequence.

4.2 Feature vectors construction of sub-sequences

To depict the form features of each subsequence, the characteristic parameters that are able to reflect the variation and distribution regularity of time series are required, such as mean value, standard deviation, skewness, and kurtosis. The mean value indicates the numerical size and centralised tendency. The standard deviation reflects the dispersion degree. Skewness describes the skew direction and degree. Kurtosis measures the steepness degree.

The time series X is segmented into M sub-sequences in the light of the identified key trend turning points, and the jth subsequence from the beginning is denoted as $X_j = [(t_k,\ x_k),\ (t_{k+1},\ x_{k+1}), \ldots, (t_{k+l-1},\ x_{k+l-1})]$, where $j = 1, 2, \ldots, M$, and $k = 1, 2, \ldots, m - l + 1$. l is the length of X_j. The characteristic parameters of X_j can be calculated as

$$\mu_j = \frac{\sum_k^{k+l-1} x_k}{l} \tag{17}$$

$$\sigma_j = \sqrt{\frac{\sum_k^{k+l-1} (x_k - \mu_j)^2}{l - 1}} \tag{18}$$

$$\mathrm{SK}_j = \frac{l\sum_k^{k+l-1}(x_k-\mu_j)^3}{(l-1)(l-2)\sigma_j^3} \tag{19}$$

$$K_j = \frac{l(l+1)\sum_k^{k+l-1}(x_k-\mu_j)^4}{(l-1)(l-2)(l-3)\sigma_j^4} - \frac{3(l-1)^2}{(l-2)(l-3)} \tag{20}$$

where μ_j, σ_j, SK_j, and K_j are the mean value, the standard deviation, skewness, and kurtosis of X_j, respectively. The four parameters constitute the feature vector of X_j, which is denoted as $\mathbf{FV}_j = [\mu_j, \sigma_j, \mathrm{SK}_j, K_j]$. Similarly, the feature vectors of other sub-sequences are determined. The time series X can be further represented as the pattern composed of feature vectors, namely $X = [\mathbf{FV}_1, \mathbf{FV}_2, \ldots, \mathbf{FV}_j, \ldots, \mathbf{FV}_M]$.

4.3 Form similarity measurement

Since the form features of each time series are various, the number of segmented sub-sequences may be different, which leads to the unequal lengths of time series composed of the feature vectors. The DTW distance is applicable to this case, but there is considerable time complexity for the calculation, while Euclidean distance is characterised by the superior computational efficiency. Therefore, FSD is designed by combining Euclidean distance and DTW distance.

For a pair of synchronous time series of the harmonic voltage amplitude U_{pcc}^h at the PCC and the harmonic emission current amplitude I_{ei}^h of harmonic source i, both of them are segmented into several sub-sequences according to the key trend turning points, and the feature vector of each subsequence is constructed. The time series U_{pcc}^h and I_{ei}^h can accordingly be expressed as

$$U_{pcc}^h = [\mathbf{FV}_1, \mathbf{FV}_2, \ldots, \mathbf{FV}_M] \tag{21}$$

$$I_{ei}^h = [\mathbf{FV}'_1, \mathbf{FV}'_2, \ldots, \mathbf{FV}'_N] \tag{22}$$

where M and N are the length of the two time series, respectively. The distance matrix $\boldsymbol{D}$ with $M \times N$ dimensions is established as (see (23)) . Every element in the distance matrix $\boldsymbol{D}$ is calculated by Euclidean distance. Considering the fact that harmonic time series mainly present certain kinds of form features in some cases, Euclidean distance is weighted to reflect the dominant position of these form features, which is expressed as

$$d(\mathbf{FV}_p, \mathbf{FV}'_q) = \sqrt{\sum_{r=1}^{4} \lambda_r(\nu_r - \nu'_r)^2} \tag{24}$$

where $d(\mathbf{FV}_p, \mathbf{FV}'_q)$ denotes the weighted Euclidean distance between the pth feature vector $\mathbf{FV}_p$ of U_{pcc}^h and the qth feature vector $\mathbf{FV}'_q$ of I_{ei}^h. $p = 1, 2, \ldots, M$, and $q = 1, 2, \ldots, N$. ν_r and ν'_r denote the rth characteristic parameter of $\mathbf{FV}_p$ and $\mathbf{FV}'_q$, respectively, where $r = 1, 2, 3, 4$. λ_r denotes the weight coefficient, which can be determined by the weighting method in [26].

Based on the principle of DTW distance, the warping path between the time series U_{pcc}^h and I_{ei}^h is searched considering the constraints of boundedness, continuity, and monotonicity [27]. As shown in Fig. 4, the shadow area represents a warping path, which is denoted as $W = [\omega_1, \omega_2, \ldots, \omega_s, \ldots, \omega_L]$ L is the length of the warping path W, and it is equal to the number of squares in the shadow area. The coordinate of the element ω_s is (p, q), which indicates the matching relation between $\mathbf{FV}_p$ and $\mathbf{FV}'_q$.

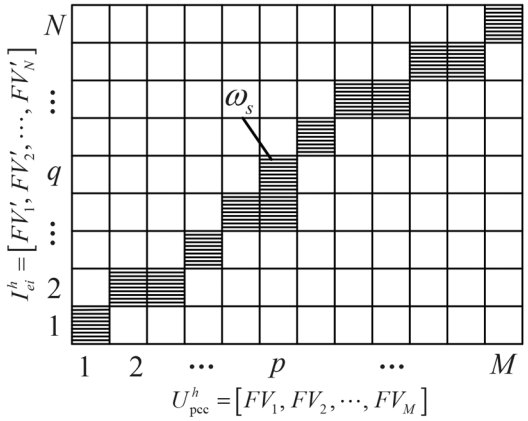

Fig. 4 *Diagram of the warping path*

There are many other warping paths such as path W that satisfies these three constraints. The ultimate goal is to find an optimal warping path to minimise the cumulative weighted Euclidean distance along the path, and the minimum distance is defined as FSD, which is expressed as

$$D_{\mathrm{FSD}}(U_{pcc}^h, I_{ei}^h) = \min \sum_{s=1}^{L} d(\omega_s) \tag{25}$$

where $D_{\mathrm{FSD}}(U_{pcc}^h, I_{ei}^h)$ denotes the FSD between U_{pcc}^h and I_{ei}^h. $d(\omega_s)$ denotes the weighted Euclidean distance between $\mathbf{FV}_p$ and $\mathbf{FV}'_q$, which is determined by (24). The solution of (25) can be derived from the dynamic programming method in [28].

4.4 Harmonic impedance calculation

For multiple pairs of time series of harmonic voltage and current amplitudes, the FSD of each pair is calculated in turn and averaged for selecting the time series with a similarity index larger than or equal to 0.9. The similarity index is defined as

$$\mathrm{SI}(j) = \frac{\bar{D}_{\mathrm{FSD}}}{\bar{D}_{\mathrm{FSD}} + D_{\mathrm{FSD}}(j)} \tag{26}$$

where $\mathrm{SI}(j)$ denotes the similarity index of the jth pair of time series. $j = 1, 2, \ldots, J$, and J is the number of time series pairs. $D_{\mathrm{FSD}}(j)$ denotes the FSD of the jth pair of time series. $\bar{D}_{\mathrm{FSD}}$ denotes the mean value of all FSDs.

The selected time series pairs are considered to have high form similarity and correspond to the relatively stable background harmonics, which enable the precise calculation of utility equivalent harmonic impedance. Then conventional linear regression methods, such as partial least squares, are competent to address the issue according to the linear correlation.

5 Harmonic contribution determination

As indicated by the above analysis, it is crucial to estimate the harmonic emission current and utility equivalent harmonic impedance for accurately determining harmonic contributions, but the harmonic coupling effect and background harmonic variations in distribution networks are major obstacles. In view of these two technical challenges, the UBSS and FSD algorithms are,

$$\boldsymbol{D} = \begin{bmatrix} d(\mathbf{FV}_1, \mathbf{FV}'_1) & \cdots & d(\mathbf{FV}_1, \mathbf{FV}'_q) & \cdots & d(\mathbf{FV}_1, \mathbf{FV}'_N) \\ \vdots & \vdots & \vdots & \vdots & \vdots \\ d(\mathbf{FV}_p, \mathbf{FV}'_1) & \cdots & d(\mathbf{FV}_p, \mathbf{FV}'_q) & \cdots & d(\mathbf{FV}_p, \mathbf{FV}'_N) \\ \vdots & \vdots & \vdots & \vdots & \vdots \\ d(\mathbf{FV}_M, \mathbf{FV}'_1) & \cdots & d(\mathbf{FV}_M, \mathbf{FV}'_q) & \cdots & d(\mathbf{FV}_M, \mathbf{FV}'_N) \end{bmatrix} \tag{23}$$

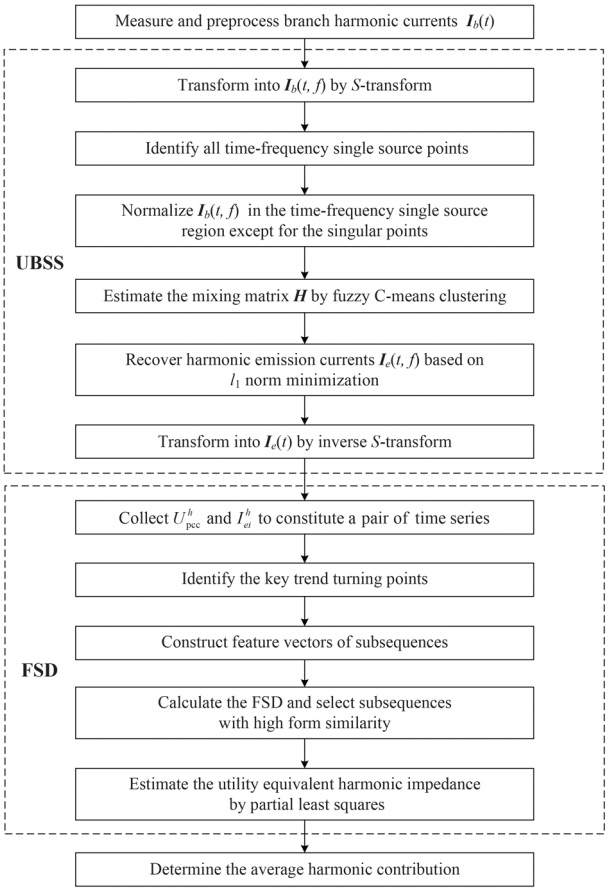

Fig. 5 *Flowchart of the proposed approach for harmonic contribution determination*

Table 1 Simulation parameters of the test system

Harmonic sources	Fundamental impedance, Ω	Fifth harmonic emission current, A
HS0	1 + j0.314	0.95∠2.2°
HS1	5 + j3.14	5.04∠-7.3°
HS2	3 + j1.57	2.05∠-12.6°
HS3	4 + j2.51	3.43∠-3.5°

respectively, adopted, and the effective quantification of harmonic contributions is further achieved. The complete procedure of the proposed approach is shown in Fig. 5.

6 Simulation study

6.1 Test system

The test system with three customer feeders shown in Fig. 1 is used to verify the performance of the proposed approach, where the utility harmonic source is denoted as HS0 and the three customer harmonic sources are denoted as HS1, HS2, and HS3, respectively. There is no necessity to adopt a more complex network for simulation analysis because the rest of the network will be equivalent to the utility harmonic source and utility harmonic impedance when studying a concerned harmonic source. The simulation study is performed on Matlab/Simulink, and the fifth harmonic is mainly considered. The specific parameters of the test system are displayed in Table 1. The normal random fluctuation with the mean value of 0 and a standard deviation of 0.1 is added to the amplitude and phase angle of the fifth harmonic emission current of each harmonic source. The simulation time is set to 40 s, and a set of the fifth harmonic voltage and current is collected as a sample every 0.02 s, so a total of 2000 samples are obtained.

6.2 Analysis of harmonic emission currents

This section is to test the UBSS-based method for harmonic emission current estimation. The utility harmonic source HS0 is assumed to be an unknown harmonic source without measurement data, and the branch harmonic currents of three customer harmonic sources are regarded as measured variables. First, the collected 2000 groups of the fifth branch harmonic currents are preprocessed, and then they are adopted to estimate the fifth harmonic emission currents of all four harmonic sources based on the proposed UBSS algorithm. Meanwhile, the fifth branch harmonic currents and the preset fifth actual harmonic emission currents are taken as the control groups for comparison.

The results are depicted in Fig. 6, which shows that the proposed UBSS-based method has a satisfactory performance in recovering source signals. The estimated values of harmonic emission currents are in good agreement with the actual values, while there is a larger deviation between the branch harmonic currents and the actual harmonic emission currents, which indicates that the branch harmonic current is unable to represent the actual harmonic emission level of harmonic sources so that it fails to reflect the true harmonic contribution.

6.3 Analysis of utility equivalent harmonic impedance

The FSD-based method, which is applied to identify stable background harmonics for the utility equivalent harmonic impedance calculation, is validated in this section. Taking HS1 as the concerned harmonic source, the background harmonic voltage at the PCC is generated by HS0, HS2, and HS3. The fifth harmonic voltage amplitudes at the PCC and the fifth harmonic emission current amplitudes of HS1 are selected to construct a pair of time series, as illustrated in Fig. 7.

Four methods are conducted to calculate the fifth utility equivalent harmonic impedance, in which method 1 is the direct partial least squares regression; method 2 is based on Euclidean distance; method 3 is based on DTW distance; method 4 is the proposed FSD-based method. Simulations are performed repeatedly 100 times to avoid the accidental calculation error, and the mean values and relative errors are shown in Table 2.

As indicated by the results, the utility equivalent harmonic impedance determined by method 1 has the largest deviation from the theoretical value, the reason for which is that the partial least squares regression is directly carried out under background harmonic fluctuations without pre-screening the harmonic voltage and current. In methods 2 and 3, the similarity search of harmonic data is conducted in advance, but the matching accuracy is not adequate due to the inherent defects of the used algorithms, which leads to the less accurate calculation results. Method 4 exhibits the optimal performance compared with the other three methods, which demonstrates that the proposed method is competent to accurately estimate the harmonic impedance with the presence of variable background harmonics.

The relative error variation of the utility equivalent harmonic impedance calculated for 100 times is displayed in Fig. 8. The result illustrates that the proposed method produces the smoothest error fluctuation, which shows better robustness than the other three methods.

6.4 Analysis of the harmonic contribution

The final step of the simulation study is to verify the effectiveness of the proposed approach for harmonic contribution determination. Five approaches are performed for comparative analysis. Approach 1 is based on the branch harmonic current and FSD. Approaches 2–5 are based on the harmonic emission current estimated by UBSS, in which approach 2 adopts the direct partial least squares regression; approach 3 uses Euclidean distance; approach 4 introduces DTW distance; approach 5 is the proposed approach.

First, the impact of harmonic source coupling on harmonic contribution determination is tested. Approaches 1 and 5 are applied to determine the fifth average harmonic contributions of HS1, HS2, and HS3, respectively. The mean values of 100 simulation results are shown in Table 3, which indicates that

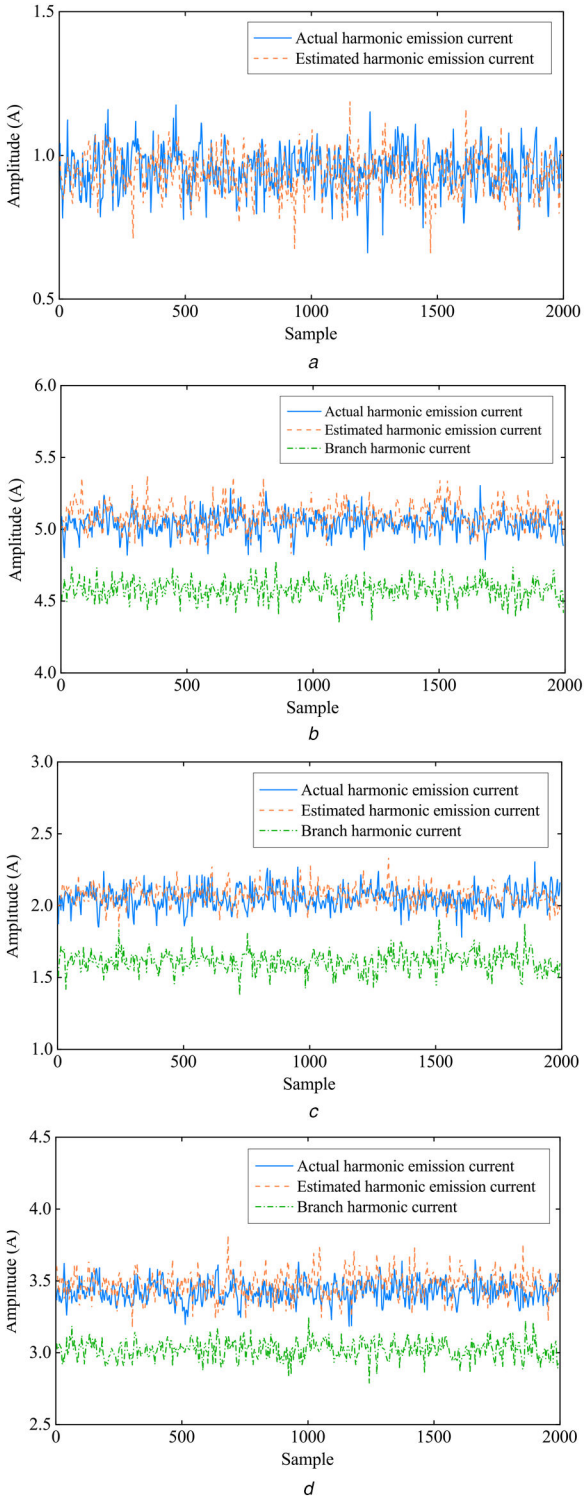

Fig. 6 *Comparison among the fifth harmonic currents of each harmonic source*
(a) HS0, ***(b)*** HS1, ***(c)*** HS2, ***(d)*** HS3

approach 5 is more accurate than approach 1 for all three harmonic sources. It is proved that the approach based on the harmonic emission current, which is obtained by the proposed UBSS algorithm, has the ability to overcome the adverse effects of harmonic source coupling and outperforms the branch harmonic current-based approach in harmonic contribution determination.

Besides, to analyse the impact of background harmonic fluctuations, approaches 2–5 are adopted to assess the fifth average harmonic contribution of HS1, respectively. The mean values and relative error variations in 100 simulation tests are depicted in Table 4 and Fig. 9, from which, it is obvious that approach 5 has the most accurate assessment result and the gentlest error

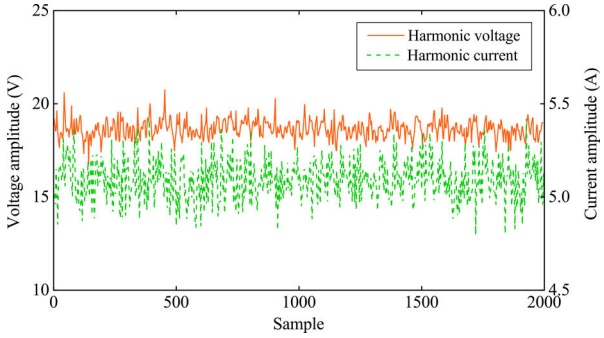

Fig. 7 *Simulation waveforms of the fifth harmonic voltage and current amplitudes*

Table 2 Calculation results of the fifth utility equivalent harmonic impedance

Method	Harmonic impedance, Ω	Relative error, %
theoretical value	2.766	—
method 1	3.265	18.04
method 2	3.136	13.38
method 3	2.553	7.70
method 4	2.662	3.76

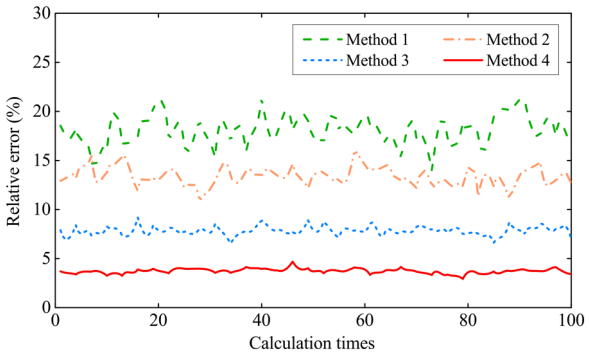

Fig. 8 *Relative errors of the utility equivalent harmonic impedance in 100 simulation tests*

Table 3 Comparison of harmonic contribution determination before and after decoupling

Approach	Harmonic contribution, %		
	HS1	HS2	HS3
theoretical value	45.31	15.87	30.04
approach 1	39.24	20.54	25.78
approach 5	43.60	13.45	32.65

Table 4 Calculation results of the fifth average harmonic contribution of HS1

Approach	Harmonic contribution, %	Relative error, %
theoretical value	75.31	—
approach 2	87.74	16.51
approach 3	84.25	11.87
approach 4	69.30	7.98
approach 5	72.46	3.78

fluctuation, indicating higher precision and stability of the proposed FSD technique.

Furthermore, the verification of the effect of background harmonic fluctuation level on harmonic contribution determination is conducted. The fifth average harmonic contribution of HS1 is evaluated while the standard deviation of the harmonic emission current fluctuation of HS0 is set to vary from 0.1 to 1. Similarly, simulations are performed repeatedly for 100 times under the

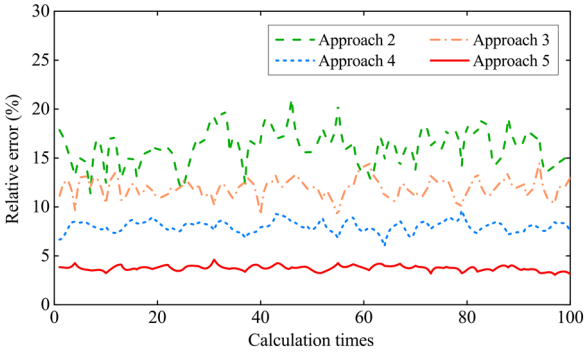

Fig. 9 *Relative errors of the average harmonic contribution of HS1 in 100 simulation tests*

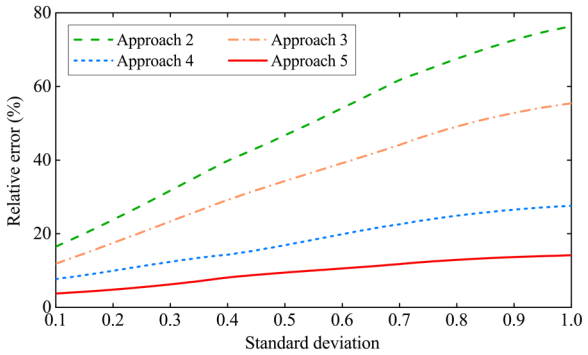

Fig. 10 *Variation trend of relative errors with the increase of background harmonic fluctuation*

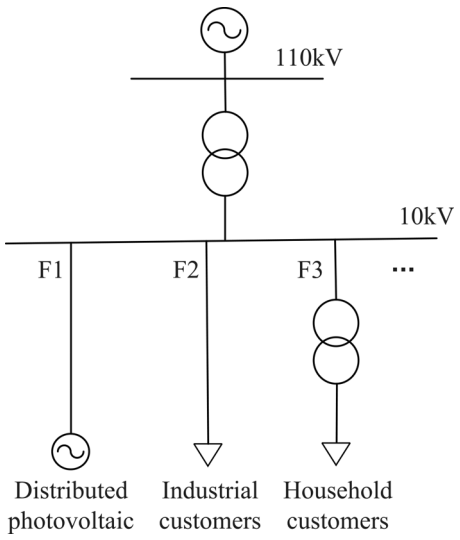

Fig. 11 *Schematic diagram of the substation*

condition of each standard deviation. Fig. 10 illustrates the variation trend of assessment errors of approaches 2–5 under different fluctuation levels, which shows that the assessment errors of approaches 2–4 increase significantly with the increase of background harmonic fluctuation, while the error of approach 5 only has a slight rise but still remain below 15%. Therefore, the proposed approach is verified to have superior performance for harmonic contribution determination even in the case of drastic background harmonic fluctuations.

7 Field measurement

To further validate the engineering applicability of the proposed approach, the field measurement is carried out at the 10 kV side in a 110 kV substation whose schematic diagram is shown in Fig. 11. The minimum short-circuit capacity of the 10 kV bus is 285 MVA, and it supplies power for a distributed photovoltaic power station, industrial customers, household customers, and so on. Other

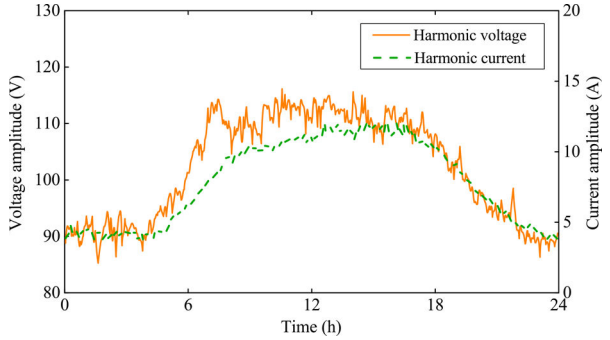

Fig. 12 *Measured waveforms of the fifth harmonic voltage and current amplitudes*

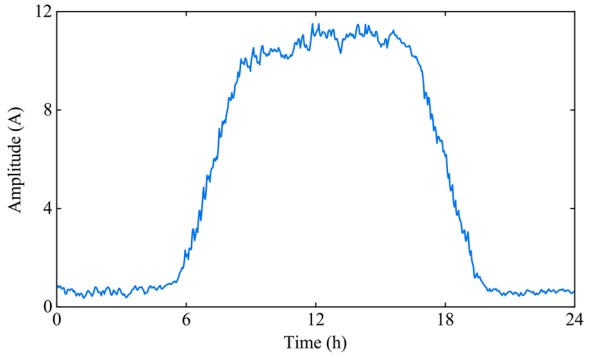

Fig. 13 *Fifth harmonic emission current of the distributed photovoltaic*

customers not shown in the figure are regarded as the background harmonic source.

The voltage of the 10 kV bus and the currents of feeders F1, F2, and F3 are synchronously collected by the BOYUU PQAny316 power quality analyser with a sampling rate of 10.24 kHz. Fast Fourier transform is applied to process the samples to acquire harmonic data, which are recorded for a continuous 24 h with a time interval of 1 min. Thus, 1440 sets of the fifth harmonic voltage and current are obtained. Fig. 12 depicts the 24-h variation trends of the fifth harmonic voltage amplitudes of the 10 kV bus and the fifth harmonic current amplitudes of feeder F1.

Based on the measurement data and short-circuit capacity of the network, the reference value of the fifth utility equivalent harmonic impedance is estimated to be 1.755 Ω, and the theoretical fifth average harmonic contribution of the distributed photovoltaic throughout the 24 h is further determined to be 14.82%.

First, the harmonic emission current estimation is conducted by the proposed UBSS algorithm. Fig. 13 indicates the fifth harmonic emission current of the concerned distributed photovoltaic over the whole day. The variation trend of the harmonic emission current is in accordance with the fact that the distributed photovoltaic operates during the daytime and is not in operation overnight. Since the level of the harmonic emission current generated by the distributed photovoltaic is low at night, its impact on the branch harmonic current is negligible, which signifies that the harmonic current on the feeder F1 at night is mainly produced by the background harmonics and it does not reflect the harmonic contribution of the distributed photovoltaic. Thus, it is confirmed that the harmonic emission current estimation through UBSS is necessary and effective.

Then through the four methods mentioned in Section 6.3, the fifth utility equivalent harmonic impedance is calculated, respectively. In a similar vein, the simulation process for each method is carried out repeatedly for 100 times to verify the accuracy and stability. The mean value and relative errors of 100 calculation results of each method are depicted in Table 5 and Fig. 14, from which the higher performance of the proposed FSD algorithm is demonstrated.

Finally, the five approaches presented in Section 6.4 are applied to evaluate the average harmonic contribution successively. In a simulation process, 1440 values of the fifth harmonic contribution

Table 5 Assessment results of the fifth utility equivalent harmonic impedance

Approach	Harmonic impedance, Ω	Relative error, %
theoretical value	1.755	—
method 1	2.894	64.90
method 2	2.378	35.50
method 3	1.422	18.97
method 4	1.631	7.07

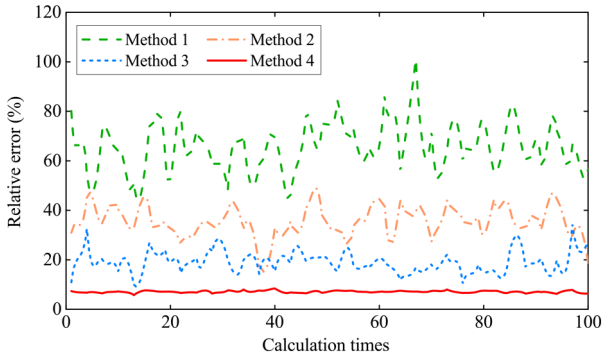

Fig. 14 *Variation trend of relative errors of the fifth utility equivalent harmonic impedance in 100 simulation tests*

Table 6 Assessment results of the fifth average harmonic contribution of the distributed photovoltaic

Approach	Harmonic contribution, %	Relative error, %
theoretical value	14.82	—
approach 1	12.87	13.16
approach 2	22.24	50.07
approach 3	18.96	27.94
approach 4	12.45	15.99
approach 5	13.79	6.95

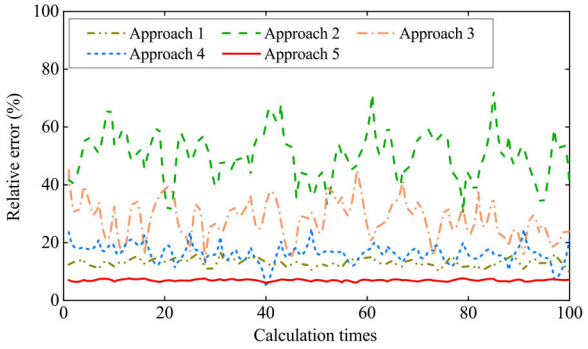

Fig. 15 *Variation trend of relative errors of the fifth average harmonic contribution in 100 simulation tests*

of the distributed photovoltaic are derived from (1), and according to (2), the fifth average harmonic contribution during the field measurement is determined. The mean value of the fifth average harmonic contributions obtained in 100 simulation tests is regarded as the assessment result of each approach, as displayed in Table 6. Besides, Fig. 15 shows the variation trend of 100 relative errors produced by each approach.

As illustrated in Table 6 and Fig. 15, since approach 1 is performed in the light of the branch harmonic current without the consideration of decoupling harmonic sources, it is inferior to approach 5 in assessment accuracy because of the deviation between the branch harmonic current and the harmonic emission current. Approaches 2–4 have insufficient ability to resist the interference of background harmonics compared with approach 5, which results in the unsatisfactory performance under significant background harmonic fluctuations. It is evident that approach 5 exhibits higher precision and robustness in multiple simulations, which indicates that the proposed approach is validated in practical applications.

8 Conclusion

This study presents a new approach to harmonic contribution determination based on UBSS and FSD. The characteristics of significant harmonic source coupling and drastic background harmonic fluctuations in modern distribution networks are taken into consideration. For the purpose of solving the two issues, the UBSS algorithm is introduced to decouple harmonic sources for harmonic emission current estimation, and the FSD algorithm is applied to decrease the undesirable effect of background harmonic variations on utility equivalent harmonic impedance calculation. As a result, the quantitative determination of harmonic contribution is performed. Through the simulation study and field measurement, the results of the comparative analysis demonstrate that the proposed approach outperforms the existing methods in terms of validity and robustness, and it is competent to be a reliable tool in practical applications. Note that the utility equivalent harmonic impedance is regarded as a constant in this study, so the further improvements need to be conducted for the impact of utility harmonic impedance variation on harmonic contributions in the near future.

9 References

[1] Tang, K., Shen, C.: 'Method for detecting harmonic responsibility misjudgements based on waveform correlation analysis', *IET Gener. Transm. Distrib.*, 2019, **13**, (9), pp. 1545–1554

[2] Zebardast, A., Mokhtari, H.: 'New method for assessing the utility harmonic impedance based on fuzzy logic', *IET Gener. Transm. Distrib.*, 2017, **11**, (10), pp. 2448–2456

[3] Liu, Q., Li, Y., Hu, S., *et al.*: 'A transformer integrated filtering system for power quality improvement of industrial DC supply system', *IEEE Trans. Ind. Electron.*, 2020, **67**, (5), pp. 3329–3339

[4] Liu, Q., Li, Y., Hu, S., *et al.*: 'A controllable inductive power filtering system: modeling, analysis and control design', *Int. J. Electr. Power Energy Syst.*, 2019, **105**, pp. 717–728

[5] Saadat, A., Hooshmand, R., Kiyoumarsi, A., *et al.*: 'Harmonic pricing in power systems based on identifying the appropriate contribution of customers', *IET Gener. Transm. Distrib.*, 2019, **13**, (1), pp. 73–80

[6] Dirik, H., Duran, I.U., Gezegin, C.: 'A computation and metering method for harmonic emissions of individual consumers', *IEEE Trans. Instrum. Meas.*, 2019, **68**, (2), pp. 412–420

[7] Xu, W., Bahry, R., Mazin, H.E., *et al.*: 'A method to determine the harmonic contributions of multiple loads'. 2009 IEEE Power and Energy Society General Meeting (PESGM), Calgary, Canada, July 2009

[8] Mazin, H.E., Xu, W., Huang, B.: 'Determining the harmonic impacts of multiple harmonic-producing loads', *IEEE Trans. Power Deliv.*, 2011, **26**, (2), pp. 1187–1195

[9] Pfajfar, T., Blazic, B., Papic, I.: 'Harmonic contribution evaluation with the harmonic current vector method', *IEEE Trans. Power Deliv.*, 2007, **22**, (1), pp. 425–433

[10] Shojaie, M., Mokhtari, H.: 'A method for determination of harmonics responsibilities at the point of common coupling using data correlation analysis', *IET Gener. Transm. Distrib.*, 2014, **8**, (1), pp. 142–150

[11] Hui, J., Yang, H., Lin, S., *et al.*: 'Assessing utility harmonic impedance based on the covariance characteristic of random vectors', *IEEE Trans. Power Deliv.*, 2010, **25**, (3), pp. 1778–1786

[12] Karimzadeh, F., Esmaeili, S., Hosseinian, S.H.: 'Method for determining utility and consumer harmonic contributions based on complex independent component analysis', *IET Gener. Transm. Distrib.*, 2016, **10**, (2), pp. 526–534

[13] Bouchard, F., Malick, J., Congedo, M.: 'Riemannian optimization and approximate joint diagonalization for blind source separation', *IEEE Trans. Signal Process.*, 2018, **66**, (8), pp. 2041–2054

[14] Bai, S., Qi, H., Xiu, N.: 'Constrained best Euclidean distance embedding on a sphere: a matrix optimization approach', *SIAM J. Optim.*, 2015, **25**, (1), pp. 439–467

[15] Deng, S., Xiang, Y., Fu, Z., *et al.*: 'A hybrid method for crude oil price direction forecasting using multiple timeframes dynamic time warping and genetic algorithm', *Appl. Soft Comput.*, 2019, **82**, pp. 1–12

[16] Zang, T., He, Z., Fu, L., *et al.*: 'Adaptive method for harmonic contribution assessment based on hierarchical K-means clustering and Bayesian partial least squares regression', *IET Gener. Transm. Distrib.*, 2016, **10**, (13), pp. 3220–3227

[17] Pourarab, M., Meyer, J., Spelko, A., *et al.*: 'Impact of variations in the utility side on the harmonic contribution of customer installations'. 2018 IEEE Power and Energy Society General Meeting (PESGM), Portland, USA, August 2018

[18] Papic, I., Matvoz, D., Spelko, A., *et al.*: 'A benchmark test system to evaluate methods of harmonic contribution determination', *IEEE Trans. Power Deliv.*, 2019, **34**, (1), pp. 23–31

[19] de Matos, E.O., Soares, T.M., Bezerra, U.H., *et al.*: 'Using linear and nonparametric regression models to describe the contribution of non-linear

loads on the voltage harmonic distortions in the electrical grid', *IET Gener. Transm. Distrib.*, 2016, **10**, (8), pp. 1825–1832
[20] Sezgin, E., Göl, M., Salor, Ö.: 'State-estimation-based determination of harmonic current contributions of iron and steel plants supplied from PCC', *IEEE Trans. Ind. Appl.*, 2016, **52**, (3), pp. 2654–2663
[21] Zhen, L., Peng, D., Yi, Z.*, et al.*: 'Underdetermined blind source separation using sparse coding', *IEEE Trans. Neur. Netw. Learn. Syst.*, 2017, **28**, (12), pp. 3102–3108
[22] Abrard, F., Deville, Y.: 'A time-frequency blind signal separation method applicable to underdetermined mixtures of dependent sources', *Signal Process.*, 2005, **85**, (7), pp. 1389–1403
[23] Hu, C., Yang, Q., Huang, M.*, et al.*: 'Diagnosis of non-linear mixed multiple faults based on underdetermined blind source separation for wind turbine gearbox: simulation, testbed and realistic scenarios', *IET Renew. Power Gener.*, 2017, **11**, (11), pp. 1418–1429
[24] Takigawa, I., Kudo, M., Toyama, J.: 'Performance analysis of minimum l1-norm solutions for underdetermined source separation', *IEEE Trans. Signal Proc.*, 2004, **52**, (3), pp. 582–591
[25] Cammarota, C.: 'Estimating the turning point location in shifted exponential model of time series', *J. Appl. Stat.*, 2017, **44**, (7), pp. 1269–1281
[26] Cai, Q., Chen, L., Sun, J.: 'Piecewise statistic approximation based similarity measure for time series', *Knowl.-Based Syst.*, 2015, **85**, pp. 181–195
[27] Sun, T., Liu, H., Yu, H.*, et al.*: 'Degree-pruning dynamic programming approaches to central time series minimizing dynamic time warping distance', *IEEE Trans. Cybern.*, 2017, **47**, (7), pp. 1719–1729
[28] Teeraratkul, T., O'Neill, D., Lall, S.: 'Shaped-based approach to household electric load curve clustering and prediction', *IEEE Trans. Smart Grid*, 2018, **9**, (5), pp. 5196–5206